Neutron Reflection from Hexadecyltrimethylammonium Bromide Adsorbed at the Air/Liquid Interface: The Variation of the Hydrocarbon Chain Distribution with Surface Concentration

J. R. Lu, M. Hromadova, E. A. Simister, and R. K. Thomas*

Physical Chemistry Laboratory, South Parks Road, Oxford OX1 3QZ, U.K.

J. Penfold

Rutherford-Appleton Laboratory, Chilton, Didcot, Oxon, U.K.

Received: February 22, 1994; In Final Form: June 16, 1994[⊗]

We have determined the structure of a monolayer of hexadecyltrimethylammonium bromide adsorbed at the air/water interface at its critical micelle concentration (9.2×10^{-4} M) and at two lower concentrations using neutron specular reflection. We have used isotopic labeling to determine the relative positions of chains, heads, and solvent, and more detailed labeling to determine the distributions of C_6 chain fragments at either end of the alkyl chains. The use of the more detailed labeling scheme has allowed us to make a quantitative estimate of the contribution of surface roughness to the structure of the layer at the three concentrations, to show that the alkyl chains are, on average, strongly tilted away from the surface normal but that the part of the alkyl chain next to the head group is less tilted. The different tilt angle distributions for the two ends of the hydrocarbon chain also indicate that there are *gauche* defects in the chain.

Introduction

We have been using neutron reflection from the air/liquid interface of solutions of the series of nonionic surfactants $C_{12}(OC_2H_4)_mOH$ (abbreviated to $C_{12}E_m$) and the series of cationic surfactants $C_nH_{2n+1}N(CH_3)_3Br$ (abbreviated to C_nTAB) to attempt to understand the structures adopted by surfactant layers adsorbed at this interface.[1-7] We have shown that isotopic labeling may be used to determine the structural relations between the three component parts of the layer: the hydrophobic chain, the hydrophilic headgroup, and the water. By further subdividing the labeling within either the headgroup or hydrophobic chain, it is possible to draw yet more detailed conclusions about the nature of the layer, particularly in relation to roughness, the orientation of the chains, and the incidence of *gauche* defects. We have so far only explored this possibility to a limited extent. In this paper, we extend the method to layers of C_{16}TAB adsorbed at the air/solution interface. We have labeled the hydrocarbon chain with six methylene groups at either end of the hydrocarbon chain, determining the distances of each fragment from the solvent and from each other. We have also used the greater sensitivity now available in neutron reflection to study the variation of these distances with surface concentration over a range of areas per molecule from 45 to 100 Å^2. Apart from the detailed labeling experiments, we have also determined the structure using the simpler labeling scheme used in our earlier work so that direct comparisons may be made between C_{16}TAB and C_{10}TAB, C_{14}TAB, and C_{18}TAB. We have previously only published a preliminary account of the C_{16}TAB structure.[8]

Experimental Details

All isotopic species of C_{16}TAB were synthesized from the appropriate hexadecyl bromide (C_{16}Br) and trimethylamine using the method previously described for C_{14}TAB.[9] The fully protonated and fully deuterated bromides, designated hC_{16}Br and dC_{16}Br, were obtained from Aldrich and K & K Greeff, respectively. The corresponding trimethylamines were from the same two sources.

The partially deuterated C_{16}Br were prepared using the Grignard coupling reaction between RBr and $Br(CH_2)_nCOOH$ to give $R(CH_2)_nCOOH$ as described previously.[2] Reduction with $LiAlH_4$ followed by bromination gave the appropriate hexadecyl bromide.[2] The compounds finally obtained were dC_6hC_{10}TAB and $hC_{10}dC_6$TAB. The chemical purity of all species of C_{16}TAB was assessed by surface tension measurements.

High-purity water was used for all the measurements (Elga Ultrapure), and the glassware and Teflon troughs for the neutron and surface tension measurements were cleaned using alkaline detergent (Decon 90) followed by copious washing in ultrapure water. Surface tension measurements were made on a Kruss K10 maximum pull tensiometer using a Pt du Nouy ring. The ring was flamed in between each measurement. All the experiments were performed at 303 K.

The neutron reflection measurements were made on the reflectometer CRISP at the Rutherford-Appleton Laboratory (Didcot, U.K.). The procedure for making the measurements has been described previously.[5] All the measurements were made at a fixed incident angle of 1.5° and the intensities calibrated with respect to D_2O. A flat background determined by extrapolation to high values of the momentum transfer, κ ($\kappa = (4\pi \sin \theta)/\lambda$ where θ is the glancing angle of incidence), was subtracted. This is a valid procedure provided that there is no small angle scattering from the bulk solution, which is generally the situation for surfactant solutions below their critical micelle concentration (cmc).

Results

Neutron reflection measurements were made at three concentrations of 9.1×10^{-4}, 2.75×10^{-4}, and 0.7×10^{-4} M. The cmc was determined from surface tension measurements

* Please address all communications to this author at: Physical Chemistry Laboratory, South Parks Rd., Oxford OX1 3QZ, U.K.

⊗ Abstract published in *Advance ACS Abstracts,* September 15, 1994.

0022-3654/94/2098-11519$04.50/0

TABLE 1: Structural Parameters of C_{16}TAB on Null Reflecting Water at the cmc (single−Layer Model)[a]

conc × 10^4 (M)	surfactant	A (Å^2)	τ (Å)	σ (Å)
9.2	dC_{16}hTAB	42 ± 2	19.5	16.4
9.2	dC_{16}dTAB	44 ± 2	21.5	18.4
9.2	hC_{16}dTAB	46	16	14 ± 2
9.2	dC_6"0"C_{10}hTAB	42	16.5	14.0
9.2	"0"$C_{10}dC_6$hTAB	42	16.4	14.0
9.2	dC_6"0"C_{10}hTAB, "0"$C_{10}dC_6$hTAB	43	20.0	18.0
2.76	dC_{16}hTAB	60	17.1	14.0
2.76	dC_6"0"C_{10}hTAB	62	14.0	11.0
2.76	"0"$C_{10}dC_6$hTAB	56	14.0	11.0
2.76	C_6"0"C_{10}hTAB, "0"$C_{10}dC_6$hTAB	57	16.0	14.0
0.70	dC_{16}hTAB	106	16.5	13.0
0.70	dC_6"0"C_{10}hTAB	95	12.0	10.0
0.70	"0"$C_{10}dC_6$hTAB	98	12.0	10.0
0.70	dC_6"0"C_{10}hTAB, "0"$C_{10}dC_6$hTAB	81	14.0	11.0

[a] τ applies to a uniform layer and σ to a Gaussian distribution (defined by eq 6).

to be 9.2 ± 0.2 × 10^{-4} M. This is within the range quoted in ref 10 and in good agreement with a recent measurement.[11] The isotopic compositions studied were dC_{16}hTAB in null reflecting water (nrw) and D_2O, "0"C_{16}hTAB in D_2O, dC_{16}dTAB in nrw, and "0"C_{16}dTAB in nrw. In addition, we measured the reflectivities of dC_6"0"C_{10}hTAB in nrw and D_2O, "0"$C_{10}dC_6$-hTAB in nrw and D_2O, and a 50:50 mixture of the two partially deuterated chain compounds in nrw. "0" designates that two isotopic species were mixed in a ratio to make the average scattering length of the appropriate part of the chain zero. We have found that this significantly increases the reflected signal when the number of protonated methylene groups is larger than the number of deuterated methylenes. For example, 10 protonated methylene groups reduces the scattering length of a dC_6-containing sample by about 20% compared with 10 "0" methylene groups. The signal is proportional to the square of the scattering length, and there is therefore a 40% increase in reflectivity. A further significant improvement is that if the level of deuteration is low, as in some of these samples, background subtraction can be a source of error. Thus the improved quality of the data in comparison with samples where the chain is fully protonated is well worth the extra effort in sample preparation.

We have shown in an earlier publication that many systematic errors in the analysis can be substantially reduced by ensuring first that the measurements are consistent with respect to surface coverage and then normalizing the set of reflectivity profiles to the average coverage.[7] A basic check on the consistency is therefore to determine the coverage from the neutron experiment by fitting a single-layer model, either a uniform layer or a Gaussian distribution, to all the data in null reflecting water. The coverage determined in this way is accurate to better than 3%, which is more than sufficient for assessing the quality of the data. The results of this analysis are shown in Table 1, and the scattering lengths used in the calculation are given in Table 2. The general level of reproducibility is better than 10% at the two higher concentrations, and with the modification of using "0" chains, it is better than 5%, but because the signal to noise decreases as the square of the surface concentration, the reproducibility at the lowest concentration is more like 15%.

A set of reflectivity profiles from samples of different isotopic composition may be analyzed in terms of the partial structure factors of the different components of the layer.[6] For the C_{16}-TAB layer, the primary features of interest are the relative positions of alkyl chains, the trimethylammonium headgroup, and water and the widths of those distributions normal to the

TABLE 2: Scattering Lengths and Volumes of Constituent Parts of C_{16}TAB[a]

unit	volume (Å^3)	extended length (Å)	scattering length (10^{-5} Å)
C_6H_{13}	185	9.1	−8.7
C_6D_{13}	185	9.1	125.9 (99.5% D)
C_6H_{12}	160	7.6	−5.0
C_6D_{12}	160	7.6	119.3 (99.5% D)
$C_{16}D_{33}$	415	21.7	324.8 (99.5% D)
$C_{16}H_{33}$	415	21.7	−17.0
$N(CD_3)_3Br$	135	–	96.2
$N(CH_3)_3Br$	135	–	2.5
D_2O	30	–	19.1
H_2O	30	–	−1.7

[a] Volumes and extended lengths are from ref 17 and scattering lengths from ref 18.

interface. Of further interest are the distributions of the labeled chain fragments, in this case, the end C_6D_{13}, which we refer to as the free hexyl group and designate as c2, and the C_6D_{12} next to the head group, which we refer to as the hexamethylene group and designate c1. The structure of the air/solution interface can then be described in terms of the distributions of the two fragments of the alkyl chains c1 and c2, the intervening C_4H_8 fragment c′, the headgroup h, and water (solvent) s. We shall only consider the subdivision of the alkyl chain at isotopic compositions where the scattering length of the c′ fragment is exactly zero and therefore partial structure factors involving this fragment are also zero and can be omitted. In terms of the remaining labels, the scattering length density can be written as

$$\varrho(z) = b_{c1}n_{c1}(z) + b_{c2}n_{c2}(z) + b_h n_h(z) + b_s n_s(z) \quad (1)$$

where n_i is the number density profile of species i and b_i is its scattering length. In terms of the partial structure factors h_{ii}, the kinematic approximation for the reflectivity $R(\kappa)$ is

$$R(\kappa) = \frac{16\pi^2}{\kappa^2}[b_{c1}^2 h_{c1c1} + b_{c2}^2 h_{c2c2} + b_h^2 h_{hh} + b_s^2 h_{ss} + 2b_{c1}b_h h_{c1h} + 2b_{c2}b_h h_{c2h} + 2b_h b_s h_{hs} + 2b_{c1}b_s h_{c1s} + 2b_{c2}b_s h_{c2s} + 2b_{c1}b_{c2}h_{c1c2}] \quad (2)$$

or, in the simpler labeling scheme,

$$R(\kappa) = \frac{16\pi}{\kappa^2}[b_c^2 h_{cc} + b_h^2 h_{hh} + b_s^2 h_{ss} + 2b_c b_h h_{ch} + 2b_c b_s h_{cs} + 2b_h h_{cs} + 2b_h b_s h_{hs}] \quad (3)$$

where h_{ij} are the partial structure factors given by

$$h_{ii}(\kappa) = |n_i(\kappa)|^2$$

$$h_{ji} = h_{ij}(\kappa) = \mathrm{Re}[n_i(\kappa)n_j{}^*(\kappa)] \quad (4)$$

where $n_i(\kappa)$ is the one-dimensional Fourier transform of $n_i(z)$, the average number density profile of atom, or group, i in the direction normal to the interface. Although it is simpler to express the reflectivity in terms of $h(\kappa)$, it is more convenient to do the analysis in terms of $h^{(1)}(\kappa)$, which is the equivalent transform in terms of the differential of the scattering length density. The two are related by

$$\kappa^2 h(\kappa) = h^{(1)}(\kappa) \quad (5)$$

The reflectivity given by eqs 2 and 3 is approximate, but as discussed by Lu et al.,[12] it can be corrected to reduce any

consequent error to a negligible level for the systems under consideration here.

There are two types of partial structure factors in eqs 2 and 3: the self-terms h_{ii} and the cross-terms h_{ij}. The self-terms can be characterized by the width, σ_i, and the amplitude, n_i, of the distribution which is in turn directly related to the surface coverage. The value obtained for the width depends on the function chosen to represent n_i. We shall use a Gaussian distribution for the surfactant fragments given by

$$n = n_{io} \exp(-4z^2/\sigma^2) \tag{6}$$

which gives

$$h_{ii}^{(1)}(\kappa) = \frac{\pi\sigma_i^2 n_{io}^2}{4}\kappa^2 \exp(-\kappa^2\sigma_i^2/8) \tag{7}$$

where n_{io} is related to the surface excess by

$$\Gamma_i = 1/A = \frac{\sigma_i n_{io}\sqrt{\pi}}{2} \tag{8}$$

For the solvent we use

$$n_s = n_o[^1/_2 + {}^1/_2 \tanh(z/\zeta)] \tag{9}$$

where z is the distance in the direction normal to the interface, ζ, is a width parameter, and n_o is the bulk number density of the solution. The corresponding partial structure factor is

$$h_{ss}^{(1)}(\kappa) = n_o^2(\zeta\pi\kappa/2)^2 \operatorname{cosech}^2(\zeta\pi\kappa/2) \tag{10}$$

The information about the relative positions of the distributions of each component is contained in the cross-partial structure factors h_{ij}. The cross-term between two distributions centered at δ_i and δ_j is[6]

$$h_{ij}(\kappa) = \mathrm{Re}[n_i(\kappa)n_j^*(\kappa) \exp[-i\kappa(\delta_i - \delta_j)]] \tag{11}$$

All distributions of fragments of the surfactant molecule are zero at large positive and negative values of z and therefore described by functions approximately symmetrical about their centers, whereas the solvent density is zero at large negative z but has its bulk value at large positive z and is therefore predominantly an odd function. When $n_c(z)$ and $n_h(z)$ are exactly even about their centers and $n_s(z)$ is exactly odd, eq 11 gives the following results[6]

$$h_{cs} = \pm(h_{cc}h_{ss})^{1/2} \sin(\kappa\delta_{cs}) \tag{12}$$

and

$$h_{ch} = \pm(h_{cc}h_{hh})^{1/2} \cos(\kappa b_{ch}) \tag{13}$$

where we have used the simpler labeling scheme of eq 3. We have discussed the errors which might arise from the assumption of oddness and evenness in the distribution functions in two previous publications.[12,13] For systems with dimensions in the range considered here, the errors are insignificant.

From a typical set of partial structure factors, e.g., the six appropriate to the simpler eq 3, six parameters, σ_c, σ_h, ζ, δ_{cs}, δ_{ch}, and δ_{hs}, are obtained by fitting eqs 7 and 10 to the self-terms and eqs 12 and 13 to the cross-terms. However, the three separations, δ_{ij}, are not independent because

$$\delta_{cs} - \delta_{ch} = \delta_{hs} \tag{14}$$

This type of relation is an important test of the consistency of the analysis. When more complicated labeling schemes are used, there may be a fair amount of redundancy in the structural parameters because of relations similar to eq 14. This redundancy is only avoidable if contrast variation may be used to eliminate completely the contribution of a fragment. In the case of C_{16}TAB with a partially labeled chain, it is possible to determine a limited set of distances because the C_4H_8 fragment may be matched exactly to air and the $N(CH_3)_3$ fragment is also almost exactly matched. Thus it is not necessary to make the several extra measurements which would be needed to determine the additional partial structure factors.

TABLE 3: Structural Parameters Obtained from Kinematic Analysis

area per molecule (Å^2):	43 ± 2	60 ± 3	100 ± 10
parameter (Å)			
σ_c	16.5 ± 1	14.0	13.0
σ_h	14.0 ± 2	10.0 ± 2	8.0 ± 3
ζ_s	6.0	5.5	5.1
δ_{cs}	9.0 ± 0.5	6.8	5.0
δ_{ch}	8.0 ± 0.5	7.0 ± 1	5.0 ± 1
δ_{hs}	2.0 ± 1	–	–
σ_{c1}	14.0 ± 2	11	10 ± 1.5
σ_{c2}	14.0 ± 2	11.0	10.0
δ_{c1s}	5.5 ± 0.5	4.0	4.0 ± 1
δ_{c2s}	12.0 ± 0.5	9.0	7.0
δ_{c1c2}	7 ± 1	5.0 ± 1	3.0 ± 1.5

For convenience, we divide the data into two sets, one giving the simpler structure according to eq 3 and the more complicated set using eq 2. We first discuss and interpret the self-partial structure factors h_{ii} obtained from the reflectivity profiles as follows. At the cmc, we used the reflectivity profiles of dC_{16}hTAB in nrw and D_2O, "0"C_{16}hTAB in D_2O, dC_{16}dTAB in nrw and D_2O, and "0"C_{16}dTAB in nrw, using eq 3, and the scattering lengths in Table 2 to obtain the six partial structure factors in eq 3. At the lower concentrations, we omitted the measurement of dC_{16}dTAB in D_2O and made the approximation that the scattering length of the protonated headgroup is zero to obtain five of the six structure factors in eq 3, the missing one being h_{hs}. Figure 1a,b shows the alkyl chain and headgroup partial structure factors h_{cc} and h_{hh} at three concentrations. The continuous lines show the fitted Gaussian distributions, using eq 7 and the parameters given in Table 3. It can be seen that there is a distinct decrease in the width of both chain and headgroup distributions with decreasing surface coverage. Both h_{cc} and h_{hh} are equally well fitted by a Gaussian distribution or a uniform layer, any difference between the two fits being within the margin of error. There is evidence from computer simulation that a Gaussian distribution is more appropriate,[12] and we have shown that a Gaussian distribution is a more accurate representation of the alkyl chain in $C_{12}E_3$.[2] We note that the most direct way of obtaining σ_i and A is to plot $\ln(h_{ii})$ against κ^2 using the logarithm of eq 7.[7]

There are two ways of determining the separations δ_{ij} from the cross-partial structure factors, either by substituting the observed h_{ii}, h_{jj}, and h_{ij} into the appropriate equation of the pair 12 and 13 or by using the Gaussians that have already been fitted to h_{ii} and h_{jj}. In the latter case, the following expression for h_{ch} can then be derived from eqs 12, 13, and 7:

$$h_{ch}^{(1)} = \frac{\kappa^2}{A^2} \exp[-\kappa^2(\sigma_c^2 + \sigma_h^2)/16]\cos\kappa\delta_{ch} \tag{15}$$

Since A, σ_c, and σ_h are already known, δ_{ch} can be determined

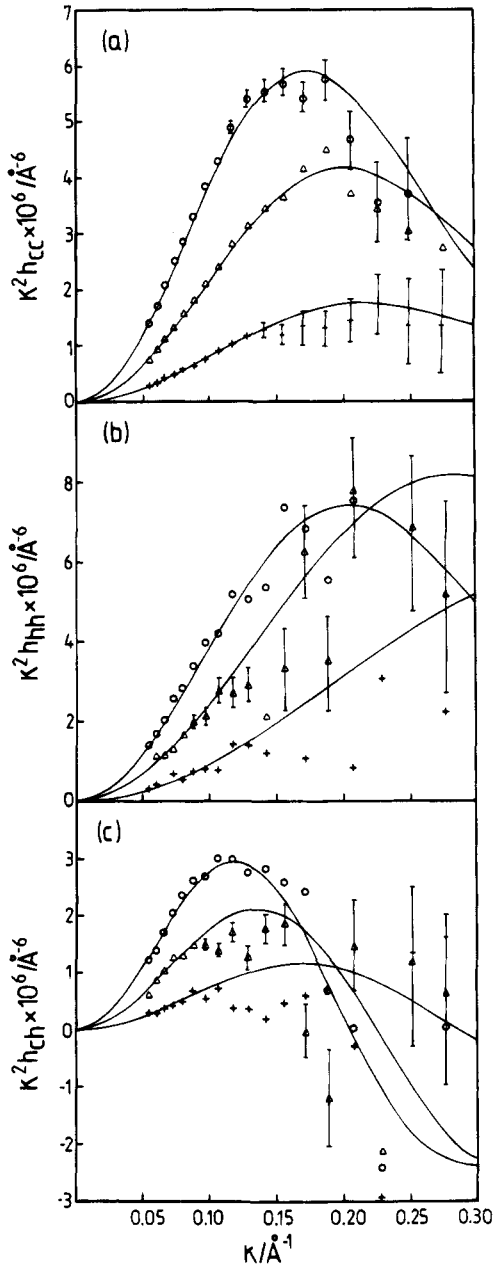

Figure 1. Partial structure factors of (a) $\kappa^2 h_{cc}$, (b) $\kappa^2 h_{hh}$, and (c) $\kappa^2 h_{ch}$ at three concentrations: 9.1×10^{-4} M (○), 2.75×10^{-4} M (△), and 0.7×10^{-4} M (+). The continuous lines in a and b are fits using Gaussian distributions with widths, σ, of (a) 16.5, 14.0, and 13.0 Å and (b) 14.0, 10.0, and 8.0 Å. Continuous lines in c are fitted as described in the text with values of δ_{ch} of 8.5, 7.0, and 5.0 Å, respectively.

directly from h_{ch}. A similar equation may be written for h_{cs} and h_{hs}, using eq 9 for the solvent, a Gaussian distribution for h_{cc} and h_{hh}, and eq 12,

$$h_{is}^{(1)} = \frac{\kappa n_o}{A} \exp[-\kappa^2\sigma_i^2/16](\zeta\pi\kappa/2)\text{cosech}(\zeta\pi\kappa/2)\sin\kappa\delta_{is} \quad (16)$$

The fits of eq 15 to $h_{ch}^{(1)}$ are shown in Figure 1c. The values of δ_{ch}, given in Table 3, vary from 8.5 to 5 Å over the concentration range studied. The fits of eq 16 to $h_{cs}^{(1)}$ are shown in comparison with the chain fragment/solvent partial structure factors in Figure 3. The values of δ_{cs} (Table 3) are similar to δ_{ch} at all three concentrations.

We now consider the set of data with partially labeled chains. Five partial structure factors were determined via eq 2 using the reflectivities of dC_6"0"C_{10}hTAB in nrw and D_2O, "0"C_{10}-

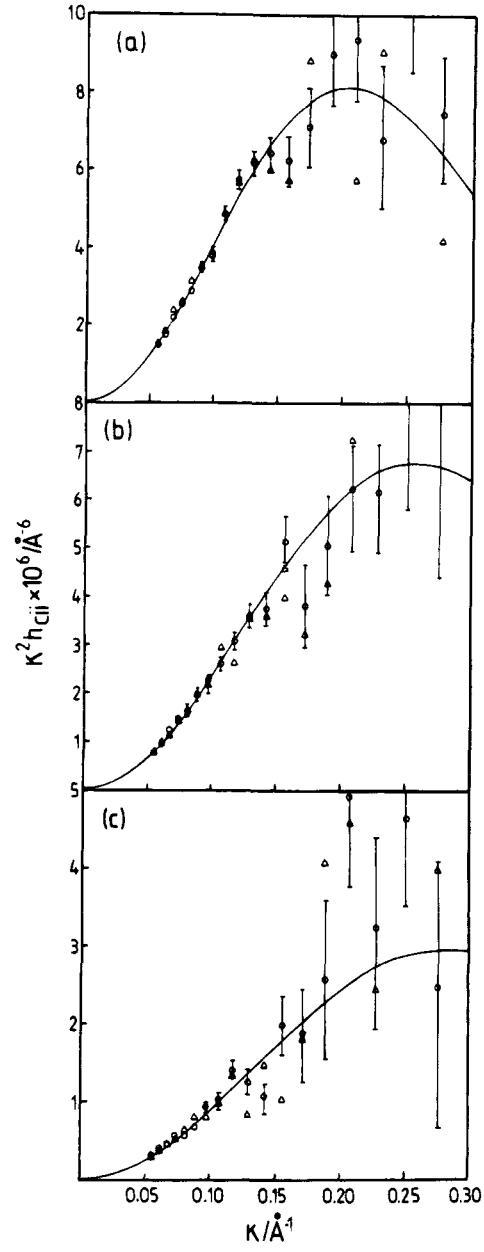

Figure 2. Partial structure factors of the hexamethylene group, $\kappa^2 h_{c1c1}$ (△), and the end hexyl group $C_6H_{13}-$, $\kappa^2 h_{c2c2}$ (○), at (a) the cmc, (b) 2.75×10^{-4} M, and (c) 7×10^{-5} M. The lines are fits for Gaussian distributions with widths of (a) 14.0, (b) 11.0, and (c) 10.0 Å.

dC_6hTAB in nrw and D_2O, and a 50:50 mixture of the two partially deuterated chain compounds in nrw with the scattering lengths given in Table 2. The headgroup scattering length was assumed to be exactly zero, and hence all the terms in eq 2 involving b_h vanish. The self-partial structure factors for the hexyl (c2) and hexamethylene groups (c1) were found to be identical within error as shown in Figure 2. Furthermore the widths, σ, given in Table 3, are only about 3 Å less than that for the whole chain (Figure 1a). At first sight this is very strange because the whole chain contains nearly 3 times as many carbon atoms, but we will show below that this is a consequence of a large roughness contribution and large angles of tilt away from the surface normal. The continuous lines in Figure 2 are the best fits of the Gaussian distribution, eq 7.

Figures 3 and 4 compare the cross-partial structure factor between each chain fragment and the solvent with that between the whole chain and the solvent at all three concentrations. The continuous lines show the best fits using eq 16, and the resulting values of δ_{cs} are given in Table 3. The comparison is done in

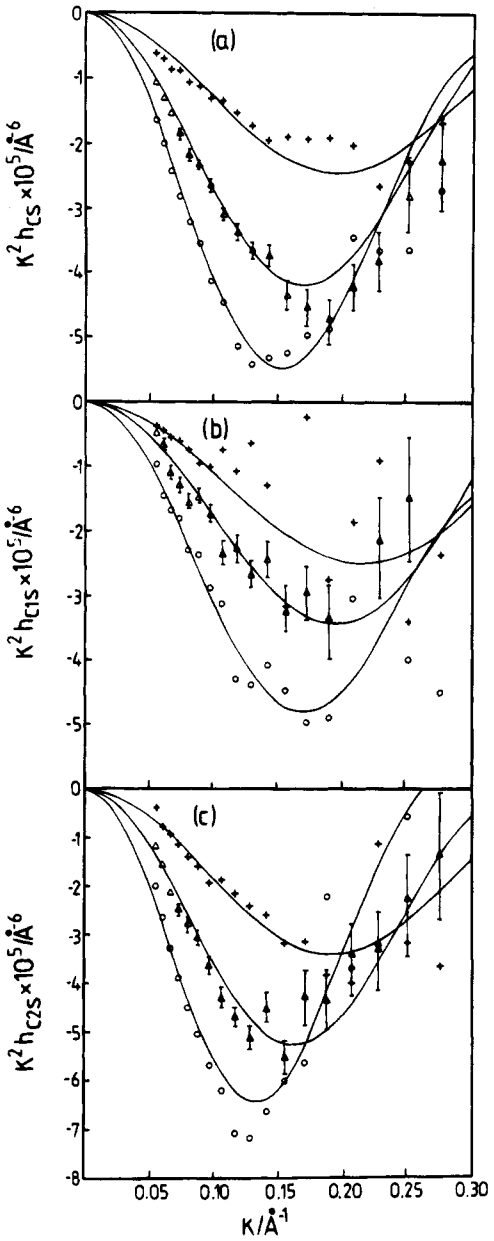

Figure 3. Cross-term partial structure factors of (a) $\kappa^2 h_{cs}$, (b) $\kappa^2 h_{c1s}$, and (c) $\kappa^2 h_{c2s}$ at three concentrations: the cmc (○), 2.75×10^{-4} M (△), and 7×10^{-5} M (+). The lines are fits of eq 16 with (a) δ_{cs} = 9.0 (○), 6.8 (△), and 5.0 Å (+), (b) δ_{c1s} = 5.5 (○), 4.0 (△), and 4.0 (+) Å, and (c) δ_{c2s} = 12.0 (○), 9.0 (△), 7.0 Å (+).

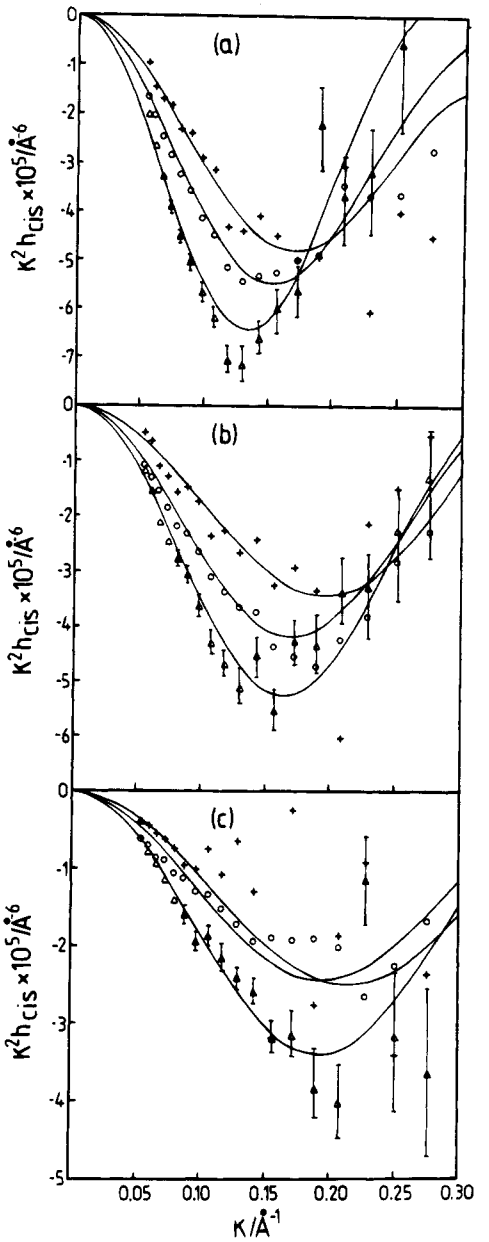

Figure 4. Cross-term partial structure factors of $\kappa^2 h_{cis}$ compared at each concentration: (a) the cmc, (b) 2.75×10^{-4} M, and (c) 7×10^{-5} M.

two ways for clarity. In Figure 3, the results are grouped according to the nature of the fragment. Thus Figure 3a shows the variation of $\kappa^2 h_{cs}$ with concentration. The decrease of δ_{cs} with concentration is clearly seen in the shift of the minimum to higher κ. Figure 4 compares the three fragments at each concentration. Thus, in Figure 4a the decrease in δ_{is} from i = the hexyl group c2 through i = the whole chain to i = the hexamethylene group c1 is again clear because of the shift of minimum to higher values of κ. Since the two C_6 groups are the same size and symmetrically disposed about the center of the C_{16} chain, δ_{cs} should be the mean of δ_{c1s} and δ_{c2s}, as is observed.

Confirmation of the disposition of the fragments in the layer is obtained by analysis of the cross-partial structure factor between the two chain fragments, $\kappa^2 h_{c1c2}$. This gives δ_{c1c2}, which should be the difference between δ_{c2s} and δ_{c1s}. This partial structure factor is shown for all three concentrations in Figure 5. The statistical quality of the partial structure factor is lower than some of the others because it is essentially obtained from the 50:50 mixture of the two partially labeled surfactants in nrw. The signal from this mixture is about 25% of what would be obtained from a C_{16}TAB sample containing both C_6 fragments fully deterated. However, the sensitivity of the data to the value of δ_{c1c2} through eq 15 is sufficiently high that the less costly method adopted here is adequate. Since there is only a relatively small change in $(h_{c1c1}h_{c2c2})^{1/2}$, the dominant contribution in eq 15 is the $\cos(\kappa\delta_{c1c2})$ term. It is then easy to discern the decrease in δ_{c1c2} with concentration in Figure 5. The values are in excellent agreement with the δ_{is} values above.

We have also used the more conventional method of fitting the data, using a model for the interfacial profile and the exact optical matrix calculation. We include the results of that analysis here because most authors still use this method for analyzing their reflectivity data, either because they do not have the range of isotopic species necessary for the partial structure factor approach or because isotope effects make such an analysis impossible. It is therefore important to include such model fits solely for the purposes of comparison with other data. The two-layer model for the interfacial profile was that used by Lu et al.[4] and consists of a region that is just alkyl chain, containing

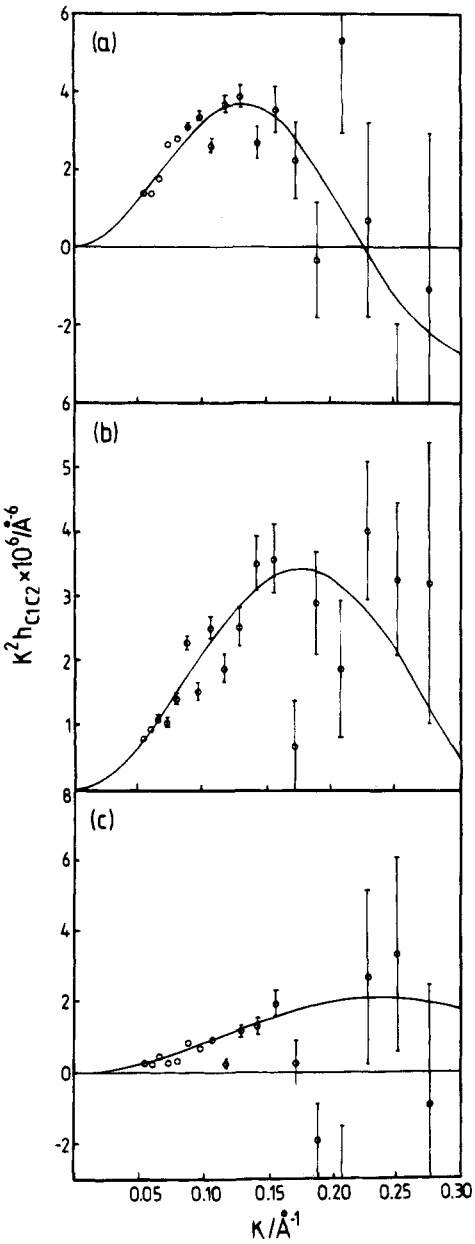

Figure 5. Partial structure factors of $\kappa^2 h_{c1c2}$ at (a) the cmc, (b) 2.75 × 10^{-4} M, and (c) 7 × 10^{-5}. The lines are fits of eq 15 with $\delta_{c1c2} = 7.0$ (a), 5.0 (b), and 3.0 Å (c).

a fraction of alkyl chains, $(1 - f_c)$, and a region containing all the headgroups and a proportion of alkyl chains, f_c, with the remaining space filled with water. There is assumed to be no water in the alkyl chain-dominated region. The results of fitting this model to the different sets of data are given in Tables 4 and 5.

Discussion

The most direct way of assessing the structure of a surfactant layer is in terms of the number distribution of the three components: alkyl chains, trimethylammonium headgroups, and water. This is compared in Figure 6 for the highest concentration with a computer simulation of $C_{16}TACl$ done at the same area per molecule by Böcker et al.[14] The agreement in the relative positions of the distributions of the three components is excellent. The simulated width of the headgroup distribution also agrees well with experiment. This is important for our further discussion below because the width of the headgroup region is much larger than would be suggested from the small size of the headgroup, and the simulation shows clearly that

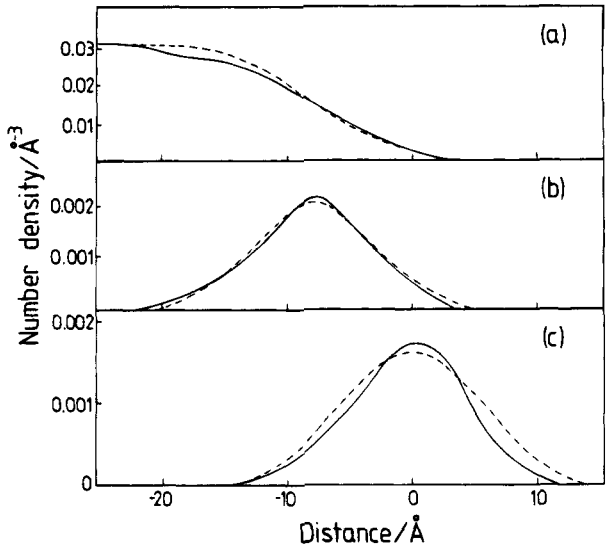

Figure 6. Comparison of experimental number density distributions (dashed lines) with those from a computer simulation (solid lines) at the cmc: (a) the solvent, (b) the headgroup, and (c) the alkyl chain.

TABLE 4: Parameters for Calculated Profiles using the Two-Layer Optical Matrix Method

conc × 10^4 (M)	A (Å^2)	$f_c \pm 0.05$	$\tau_c \pm 1$ (Å)	$\tau_h \pm 1$ (Å)	$n \pm 1$
9.2	43 ± 3	0.30	12.0	10.5	6
2.76	60 ± 4	0.35	10.5	9.5	9
0.70	100 ± 10	0.40	9.0	8.5	13

roughness makes an important contribution to this width. The only disagreement between simulation and experiment is that the experimental chain width is greater by about 25%, comfortably outside the experimental error on the basis of the assumption that the distribution is Gaussian. It is almost certainly also outside any errors arising from deviations of the real distribution from Gaussian. Thus the distribution from the computer simulation is slightly skewed but not to an extent that inclusion of this skewness would have a significant effect on the fitted width. It is difficult to be sure what is the origin of the discrepancy. The weakest points in the simulation are likely to be the assumed potential between CH_2 fragments on different molecules and the effect of capillary waves. The roughness induced by the capillary waves, which is clearly seen in the simulation of Böcker et al., must be coupled to the tilt angles of the molecules and the incidence of *gauche* defects, both of which will affect the thickness of the chain region of the layer. It is not clear how the lateral dimensions of the sample used for the simulation will affect the capillary wave spectrum, but there may be further contributions to the roughness from even longer wavelength capillary waves.

An alternative way of representing the structure of the monolayer is in terms of the volume fraction distributions. This shows more clearly how much space each component occupies and also gives a consistency test for the structure in that the total volume fraction at any point in the layer should not exceed the space-filling limit of unity. We show the distributions in this form for the highest and lowest concentrations in Figure 7. Features worthy of note are that the widths of the $N(CH_3)_3$ head and the two much longer C_6 fragments have similar width distributions at each concentration. This has to mean that the width of each of the three distributions is dominated by the effects of roughness. This conclusion is supported by the fact that the width of the whole chain (16.5 Å at the highest surface concentration) is only slightly larger than the width of the headgroup and individual C_6 fragments (14 Å). An estimate of the contribution of roughness to the width may be made from the data as described below.

TABLE 5: Parameters Calculated for the Profiles Measured from Surfactants with Partially Labeled Alkyl Chains using the Two-Layer Optical Matrix Method[a]

conc × 10^4 (M)	system	$A \pm 3$ (Å^2)	$f_c \pm 0.05$	$\tau_c \pm 1$ (Å)	$\tau_h \pm 1$ (Å)	$n \pm 1$
9.2	dC_6"0"C_{10}hTAB/nrw	42	0.10	12.0	10.5*	–
9.2	dC_6"0"C_{10}hTAB/D_2O	41	0.10	12.0	10.8	6
9.2	"0"$C_{10}dC_6$hTAB/nrw	42	0.60	7.0*	10.5	–
9.2	"0"$C_{10}dC_6$hTAB/D_2O	43	0.60	7.0*	10.5	6
9.2	dC_6"0"C_{10}hTAB, "0"$C_{10}dC_6$hTAB/nrw	43	0.30	12.0	10.0	–
2.76	dC_6"0"C_{10}hTAB/nrw	61	0.05	10.5	7.0*	–
2.76	dC_6"0"C_{10}hTAB/D_2O	60	0.05	11.0	10.0	9
2.76	"0"$C_{10}dC_6$hTAB/nrw	56	0.60	6.0*	9.5	–
2.76	"0"$C_{10}dC_6$hTAB/D_2O	60	0.60	7.0*	9.5	9
2.76	dC_6"0"C_{10}hTAB, "0"$C_{10}dC_6$hTAB/nrw	57	0.35	10.5	9.5	–
0.70	dC_6"0"C_{10}hTAB/nrw	95	0.05	9.0	1.5*	–
0.70	dC_6"0"C_{10}hTAB/D_2O	100	0.05	9.0	8.5	13
0.70	"0"$C_{10}dC_6$hTAB/nrw	90	0.60	4.0*	8.5	–
0.70	"0"$C_{10}dC_6$hTAB/D_2O	89	0.60	4.0*	8.5	13
0.70	dC_6"0"C_{10}hTAB, "0"$C_{10}dC_6$hTAB/nrw	83	0.40	9.0	8.5	–

[a] An asterisk denotes that fitting is not sensitive to the parameter at the particular contrast.

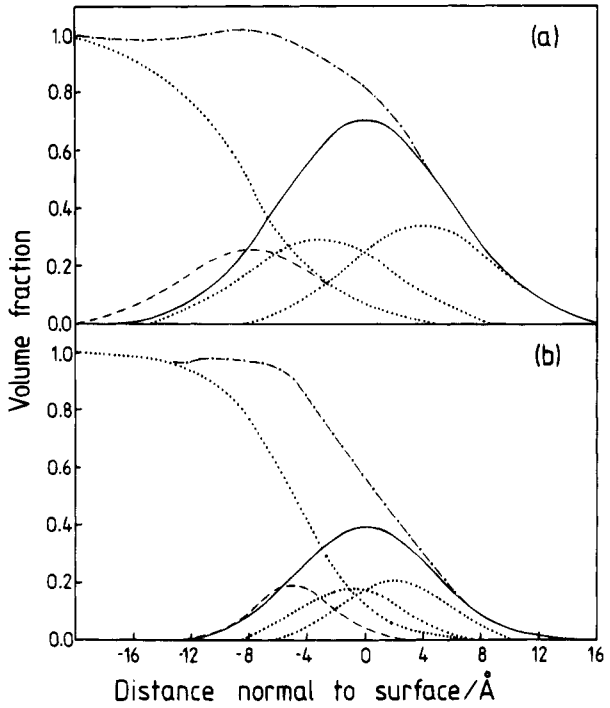

Figure 7. Experimental volume fraction distributions of the different components of a layer of $C_{16}TAB$ at the air/water interface at concentrations of (a) the cmc and (b) 7×10^{-5} M. Solid lines represent the alkyl chain, dashed lines the headgroup, dotted lines the water, and dashed–dotted lines the total volume fraction. The two chain fragments are also shown as dotted lines. All the width parameters are given in Table 3.

The structural parameters that have been obtained by the direct analysis are of two types, widths (σ) and separations (δ). There are three contributions to the width σ of any fragment of the layer: the roughness of the surface, which is a combination of either or both static disorder and thermal fluctuations (capillary waves), the mean tilt of the fragment with respect to the surface normal, and the incidence of *gauche* conformations in the fragment. The mean tilt of the fragment and the incidence of *gauche* conformations within it are combined into the mean projection of the length of the fragment on to the surface normal direction, given by

$$\langle l_z \rangle = \langle l \cos \theta \rangle \simeq \langle l \rangle \langle \cos \theta \rangle \qquad (17)$$

where $\langle l \rangle$ is the mean end-to-end length of the fragment and $\langle \cos \theta \rangle$ is the mean tilt, and the final result assumes that the two are not correlated. For Gaussian distributions, the observed

TABLE 6: Ratio of Experimental to Maximum Separations of Fragments in the Layer

		δ/l_e		
fragments	l_e	$A = 43$ Å^2	$A = 60$ Å^2	$A = 100$ Å^2
$C_{16}H_3$/head	12.6	0.64 ± 0.03	–	–
$C_{16}H_{33}$/solvent[a]	12.6	0.64 ± 0.03	0.55 ± 0.1	0.4 ± 0.1
C_6H_{13}/solvent[a]	18.9	0.58 ± 0.02	0.48 ± 0.05	0.37 ± 0.05
C_6H_{13}/C_6H_{12}	13.35	0.52 ± 0.08	0.4 ± 0.1	0.2 ± 0.15
C_6H_{12}/solvent[a]	5.55	0.8 ± 0.1	0.7 ± 0.1	0.7 ± 0.1

[a] At the highest concentration, the ratio is calculated by allowing for the solvent being 1 Å further from the chains than the headgroup; at the other two concentrations, it is assumed that solvent and headgroup distributions coincide.

width σ of the resulting convolution of the two distributions is given by

$$\sigma^2 = \langle l_z^2 \rangle + w^2 \qquad (18)$$

where w accounts for all contributions to the roughness and

$$\langle l_z^2 \rangle = \langle l^2 \cos^2 \theta \rangle \simeq \langle l^2 \rangle \langle \cos^2 \theta \rangle \qquad (19)$$

where eq 18 assumes that there is no correlation of l_z and w and eq 19 assumes l and cos θ to be uncorrelated. The values of the separations between different fragments are not affected by the surface roughness. They are determined only by an equation similar to eq 17 but with l and θ replaced by l_{ij} and θ_{ij}, the length and tilt of the vector joining the midpoints of the two fragments, i.e.,

$$\delta_{ij} = \langle l_{ijz} \rangle = \langle l_{ij} \cos \theta_{ij} \rangle \simeq \langle l_{ij} \rangle \langle \cos \theta_{ij} \rangle \qquad (20)$$

The measured δ values may be used in conjunction with the assumption that the chain or the chain fragments are fully extended to estimate $\langle \cos \theta_{ij} \rangle$. The maximum possible value of the distance between the centers of two fragments, l_c, is the distance taken along the fully extended chain. These values are given in the second column of Table 6, where we have taken the length of the headgroup to be 2.5 Å but its scattering length center of gravity to be 1.75 Å from the α-CH_2 (methylene group next to the headgroup). The values of δ/l_e are then the values of $\langle \cos \theta_{ij} \rangle$ with the assumption that $l_e = l_{ij}$, an assumption which will become increasingly valid as the chain fragment shortens. The most complete and accurate set of data is that for the highest surface concentration. These show a clear pattern, $\langle \cos \theta_{ij} \rangle$ for the C_6H_{12} nearest the solvent having the highest value, showing that this group is least tilted away from the surface normal. If the tilt angle were fixed, this value of cos θ would correspond

TABLE 7: Calculation of Roughness Parameters (Å)

fragment	$A = 43$ Å^2	$A = 60$ Å^2	$A = 100$ Å^2
	From Eq 18 and Table 6		
chain/solvent	9	7.5	9.5
C_6H_{13}/solvent	13	10	9.5
C_6H_{13}/C_6H_{12}	–	–	–
C_6H_{12}/solvent	14	9	8.5
	From Surface Tension		
	9.0	7.4	6.7

to a tilt of about 30° away from the normal. The remaining fragments are more strongly tilted with values of $\langle \cos \theta_{ij} \rangle$ in the region of 0.6 at the highest concentration, which for a single tilt angle would correspond to about 50°.

The contribution of roughness to the layer may be estimated approximately as follows. We use eq 18 taking $\langle l_z^2 \rangle$ to be identical with δ^2 where δ corresponds to the appropriate length and is obtained from the experiment (Table 6). The approximation results from the different effects of averaging $\cos \theta$ and $\cos^2 \theta$, as can be seen from eqs 19 and 20. However, as the fragment being studied decreases in size, the contribution of $\langle l_z^2 \rangle$ in eq 18 becomes less and σ^2 is increasingly dominated by the roughness, w^2. The values thus obtained for w are given in Table 7. The values for the smaller distances agree tolerably well and indicate a large roughness of the layer. The value of the roughness obtained by considering the whole chain is smaller but, for the reasons given above, is considered to be less reliable.

A separate estimate of the surface roughness assumes that it is entirely attributable to capillary waves and that these are the same as for a pure liquid at the corresponding surface tension. Schwartz et al.[15] have used X-ray reflection to study the amplitude of capillary waves on water, and the general effect of surface tension on the capillary wave spectrum is well-known theoretically.[16] Depending on the resolution of the experiment, there is a cutoff point in the wave vector of the capillary waves. Those with wave vectors smaller than the resolution cutoff are part of the specular reflection, and those with larger wave vectors are scattered away from the specular direction and contribute to the background. The reflectivity is reduced by $\exp(-\kappa^2\sigma^2)$, where σ is the mean square roughness, which is 2.8 Å for clean water. The effect of surface tension on this roughness can be estimated from

$$\langle \sigma^2 \rangle = \frac{kT}{4\pi\gamma} \ln\left[\frac{1 + 2(\pi a/l)^2}{1 + 2(\pi a/L)^2}\right] \qquad (21)$$

where a is the capillary length (0.4 cm for water), L is a length determining the resolution cutoff of the experiment, and l determines the high wave vector cutoff and is often taken to be the diameter of the molecule. The dominant term is the surface tension γ and we can therefore estimate the contribution of the thermal motion to w by taking the appropriate value of the surface tension of the C_{16}TAB solution. At the cmc, we obtain $\sigma \simeq 3.9$ Å, and at 7×10^{-5} M, $\sigma \simeq 2.9$ Å. These are not the appropriate values to use in eq 18 because they are separated by a Fourier transform, which requires σ to be multiplied by about 2.3 to obtain the values of w given in Table 7.

Taking the average of the larger estimates of w in Table 7 gives a value greater than the calculated capillary wave value, which indicates that there may be some "static" roughness. Using the quadrature formula (eq 18), the noncapillary wave roughness is about 9 Å at the cmc. We note also that the total roughness at the cmc accounts for most of the observed thickness of the headgroup region. After removal of this roughness, the headgroup thickness is about 6 Å, which is comparable with the expected dimensions of the trimethylammonium bromide group.

The reflection experiments on labeled C_{16}TAB have identified a number of features of the layer, which may be summarized as follows:

(i) it is rougher than would be predicted from a simple capillary wave model,

(ii) overall the chains are strongly tilted away from the surface normal,

(iii) the tilt away from the surface normal becomes greater as the surface concentration is reduced,

(iv) different parts of the chain have different average tilts, showing that there are *gauche* defects in the alkyl chain, and

(v) that part of the chain closest to the water (first six carbon atoms) is closer to a vertical orientation than any other part of the hydrocarbon chain.

Although there is one discrepancy with a recent computer simulation,[14] the overall picture of a layer highly disordered with respect to orientation, *gauche* defects in the chain, and vertical position is substantiated. To make further progress toward making a more quantitative characterization of the frequency of incidence of *gauche* defects in the chains and the distribution of orientations will require higher resolution determination of the structure of the layer. This can be achieved by using labeling schemes where the chain is more subdivided than in the present work, and we are currently attempting such experiments.

Acknowledgment. We thank the Science and Engineering Research Council for support. E.A.S. thanks Unilever p.l.c. for contribution to her studentship. M.H. thanks the Soros Foundation for a scholarship.

References and Notes

(1) Lu, J. R.; Lee, E. M.; Thomas, R. K.; Penfold, J.; Flitsch, S. L. *Langmuir* **1993**, *9*, 1352.
(2) Lu, J. R.; Hromadova, M.; Thomas, R. K.; Penfold, J. *Langmuir* **1993**, *9*, 2417.
(3) Lu, J. R.; Li, Z. X.; Su, T. J.; Thomas, R. K.; Penfold, J. *Langmuir* **1993**, *9*, 2408.
(4) Lu, J. R.; Li, Z. X.; Thomas, R. K.; Staples, E. J.; Tucker, I.; Penfold, J. *J. Phys. Chem.* **1993**, *97*, 8012.
(5) Lee, E. M.; Thomas, R. K.; Penfold, J.; Ward, R. C. *J. Phys. Chem.* **1989**, *93*, 381.
(6) Simister, E. A.; Lee, E. M.; Thomas, R. K.; Penfold, J. *J. Phys. Chem.* **1992**, *96*, 1373.
(7) Lu, J. R.; Simister, E. A.; Thomas, R. K.; Penfold, J. *J. Phys. Chem.* **1993**, *97*, 6024.
(8) Lu, J. R.; Hromadova, M.; Simister, E. A.; Thomas, R. K.; Penfold, J. *Physica B* **1994**, *6*, A403–A408.
(9) Simister, E. A.; Thomas, R. K.; Penfold, J.; Aveyard, R.; Binks, B. P.; Cooper, P.; Fletcher, P. D. I.; Lu, J. R.; Sokolowski, A. *J. Phys. Chem.* **1992**, *96*, 1383.
(10) *Critical Micelle Concentrations of Aqueous Surfactant Systems*; Mukerjee, P., Mysels, K. J., Eds.; National Standard Reference Data System-National Bureau of Standards 36, 1971.
(11) Aveyard, R.; Cooper, P.; Fletcher, P. D. I. *J. Chem. Soc., Faraday Trans.* **1990**, *86*, 3623.
(12) Lu, J. R.; Simister, E. A.; Lee, E. M.; Thomas, R. K.; Rennie, A. R.; Penfold, J. *Langmuir* **1992**, *8*, 1837.
(13) Simister, E. A.; Lee, E. M.; Thomas, R. K.; Penfold, J. *Macromol. Rep.* **1992**, *A29*, 147.
(14) Bocker, J.; Schlenkrich, M.; Bopp, P.; Brickmann, J. *J. Phys. Chem.* **1992**, *96*, 9915.
(15) Schwartz, D. K.; Schlossman, M. L.; Kawamoto, E. H.; Kellogg, G. J.; Pershan, P. S.; Ocko, B. M. *Phys. Rev.* **1990**, *A41*, 5687.
(16) Levich, V. *Physicochemical Hydrodynamics*; Prentice Hall: NJ, 1962.
(17) Tanford, C. J. *J. Phys. Chem.* **1972**, *76*, 3020.
(18) Sears, V. F. *Neutron News* **1992**, *3*, 26.